Collective Dislocation Behaviour in Dilute Alloys and the Portevin–Le Châtelier Effect

Y. Estrin* and L.P. Kubin**

*Technical University Hamburg–Harburg, 21 Hamburg 90, FRG

**LEM, CNRS–ONERA (OM), B.P.72, 92322 Châtillon Cedex, France

Abstract

The Portevin–Le Châtelier effect is discussed in terms of a model based on behaviour of crystal lattice defects. The model integrates two aspects of this behaviour: dynamic strain ageing associated with solute diffusion to dislocations and evolution of the densities of mobile and forest dislocations. The association of the PLC effect with the condition that the strain rate sensitivity of the flow stress be negative is demonstrated by linear stability analysis. It is further shown that plastic strain rate at a given specimen site undergoes relaxation oscillations in time keeping the average at the value prescribed by the imposed deformation (or loading) conditions. All characteristics of temporal behaviour can be found from the model. It is shown that this behaviour gives rise to a spatial pattern whose features can be investigated numerically provided the band propagation velocity is known. The importance of studying this quantity is emphasized.

1. Introduction

If one were to look for evidence of localized plastic deformation, there perhaps wouldn't be a better example than the Portevin–Le Châtelier (PLC) effect. The effect consists in repeated generation and propagation of deformation bands in a tensile specimen. These manifest themselves in discontinuities ("serrations") on deformation curves

(Fig. 1) and sometimes can be visualized on the specimen surface (Fig. 2). The understanding of the PLC effect advanced significantly in the last decade or so, and a summary of the state–of–the–art appears timely at this stage.

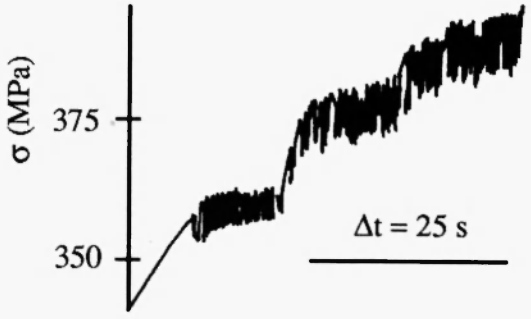

Fig. 1. A fragment of stress vs. time diagram for Al–5%Mg exhibiting PLC serrations under constant strain rate of $5 \cdot 10^{-4}$ s^{-1}.

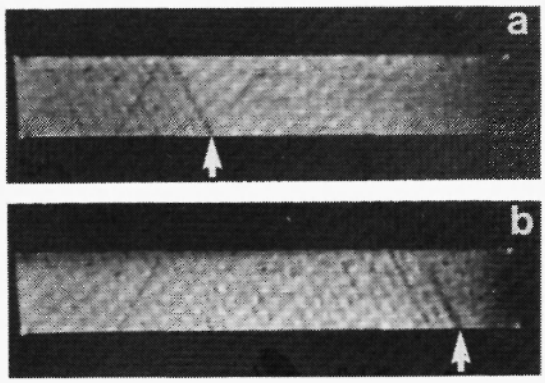

Fig. 2. Surface markings associated with PLC band propagation in Al–5%Mg under constant strain rate of $5 \cdot 10^{-4}$ s^{-1}.

The experimental situation with regard to the PLC effect is reviewed by Neuhäuser in this volume [1]. Various aspects of the phenomenon have been surveyed earlier by Kocks [2], Strudel [3], Rodriguez [4], and Pink and Grinberg [5]. In the present article, we undertook to overview the field, while concentrating on the theoretical description.

The investigation of the PLC effect has a long record. It has first been discovered by Le Châtelier in 1909 on mild steels at a slightly elevated temperature [6] and has been found later (1924) by Portevin and Le Châtelier on duraluminium alloys at room temperature [7]. As a matter of fact, the so called blue–brittleness of steels – a phenomenon related to the PLC effect – has been observed by Adamson as early as in 1878 (see quotation in Ref. 8). Since then, the PLC effect has been recorded in a number of dilute alloys (both substitutional and interstitial) of Al, Cu, Ni, Fe, Mg, etc. (in polycrystalline form for the most part). The phenomenology of the PLC effect may be quite complex, e.g. due to interference of such processes as precipitation, formation of the Guinier–Preston zones, etc. [9]. It can be considered established, however, that a negative strain rate sensitivity of the flow stress is a necessary prerequisite for the occurrence of the PLC effect [2,10–13]. Consequently, this is a central feature of the approach outlined below.

Negative strain rate sensitivity (SRS) of the flow stress is one of macroscopic manifestations of dynamic strain ageing (DSA). The underlying microscopic mechanism of DSA is additional pinning of mobile dislocations, temporarily arrested on localized obstacles, by solute atoms. Since solute diffusion is involved, DSA can only be effective within a certain range of temperature T and plastic strain rate $\dot{\epsilon}$. The domain of DSA is generally broader than that of the PLC effect, and the proximity of the latter is usually felt by such attributes as a hump on the flow stress vs. temperature diagram, a SRS dip and a ductility hole in the corresponding range of T and $\dot{\epsilon}$. The PLC effect proper occurs within a well–defined area in the $(T,\dot{\epsilon})$ plane. Moreover, for a given temperature and a fixed strain rate from within this area, a certain critical conditions involving plastic strain have to be fulfilled for discontinuous deformation to occur. This is seen from the fact that the onset of the PLC effect often requires an incubation strain, $\epsilon_c = \epsilon_c(T,\dot{\epsilon})$. Sometimes, there is, in addition, an upper critical strain so that only a limited portion of a stress–strain curve is serrated. More complex behaviour has been observed occasionally (see

below). A theory of the PLC effect has, of course, to account for the occurrence of the critical strains as well as for their temperature and strain rate dependences observed.

In the present study, we outline a model which explains the features described above. It is based on a constitutive equation whose mathematical form gives rise to an instability of continuous uniform deformation with the properties sought for. In Section 2, microscopic mechanisms leading to this mathematical form are discussed. These involve (i) dynamic interaction of solutes with temporarily arrested mobile dislocations via some diffusional process (possibly including reordering of atoms within dislocation cores) and (ii) collective dislocation effects associated with the evolution of two dislocation populations: mobile and forest dislocations. A synthesis of these two aspects leads to an expression for the intrinsic SRS. This expression serves as a basis for analysis of the mechanism of instabilities and temporal variation of the corresponding mechanical response (Section 3). In Section 4, various consequenses of the model, especially with regard to strain and strain rate effects, are discussed in connection with experimental data. Finally, Section 5 deals with some unsolved problems, in particular, with those related to spatial aspects of strain localization.

2. Dynamic strain ageing and the intrinsic strain rate sensitivity

Theories of the PLC effect are based on the interaction of mobile dislocations with solute atoms. The approach goes back to Cottrell [14] and Friedel [15]. While continuous viscous motion of dislocations was considered in these early models, a discontinuous character of dislocation motion was taken into account in later treatments [16,17]. In these, the interaction between solute atoms and dislocations held by localized obstacles was considered responsible for additional glide resistance which decreases with decreasing waiting time at an obstacle, i.e. with increasing strain rate. A consequence of this process

underlying dynamic strain ageing is a reduced strain rate sensitivity of the flow stress. The PLC effect is thought to be associated with the SRS getting negative.

2.1 Basic mechanisms

The stress σ to move a dislocation in its glide path can be assumed to be additively made up of two contributions. One, denoted σ_d, stems from the interaction of the dislocation with the dislocation ensemble, primarily with forest dislocations. The other, referred to as the "friction stress" f, originates from interactions between the mobile dislocations and solute atoms. One has [2]

$$\sigma = \sigma_d + f \tag{1}$$

The dislocation contribution, σ_d, can, in turn, be decomposed into an athermal part σ_d^a and a component σ_d^{th} originating from interactions of mobile dislocations with localized obstacles – forest dislocations. Overcoming these obstacles is considered to be a thermally activated process. Regrouping the terms, eq. (1) can be rewritten as

$$\sigma = \sigma_d^a + F \tag{2}$$

where

$$F = \sigma_d^{th} + f. \tag{3}$$

The term F is a function of temperature and disloction velocity v, while σ_d^a is largely independent of these quantities. It does evolve with strain, however. In a "usual", i.e. non–dynamic strain ageing material, F increases with v and decreases with T, in accordance with an Arrhenius relation connecting these quantities. For a dynamic strain ageing material, F turns out to decrease with v in a certain range of dislocation velocities. This "anomaly" results from the behaviour of the friction stress f which can be qualitatively described as follows. At small velocities, solute atoms have enough time to diffuse to temporarily arrested dislocations (or to get redistributed near dislocation junctions)

thus impeding the breakaway from localized obstacles. In the opposite limit case of high velocities, such additional pinning is suppressed, for the dislocattion waiting time at localized obstacles is too short for the diffusional processes to be operative. The two velocity ranges are characterized by different slopes (different "friction coefficients") in the f vs. v curve: large in the low velocity range where mobile dislocations have to drag along their solute atmospheres and small in the high velocity range where they are free from solute atmospheres (Fig. 3a). It is the velocity range in between where a negative dependence of f on v occurs. The function $F(\dot{\epsilon})$ (Fig. 3b) retains a characteristic shape of

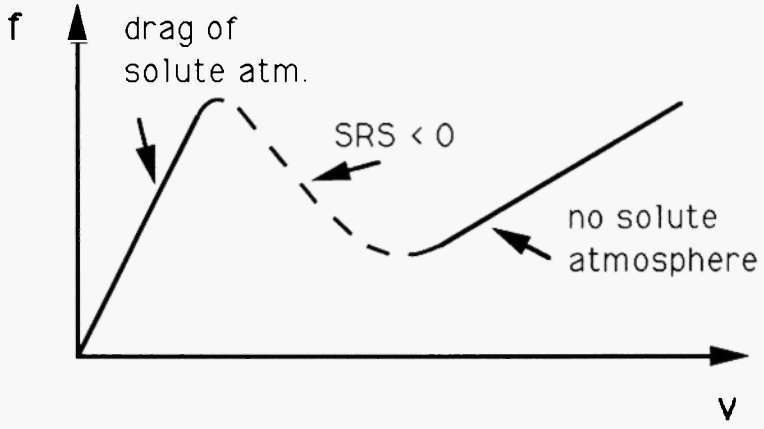

Fig. 3. Thermal component of stress in a dynamic strain ageing alloy (schematic).
(a) "Friction stress" f as a function of dislocation velocity v. The dotted portion of the curve gives rise to a negative strain rate sensitivity.

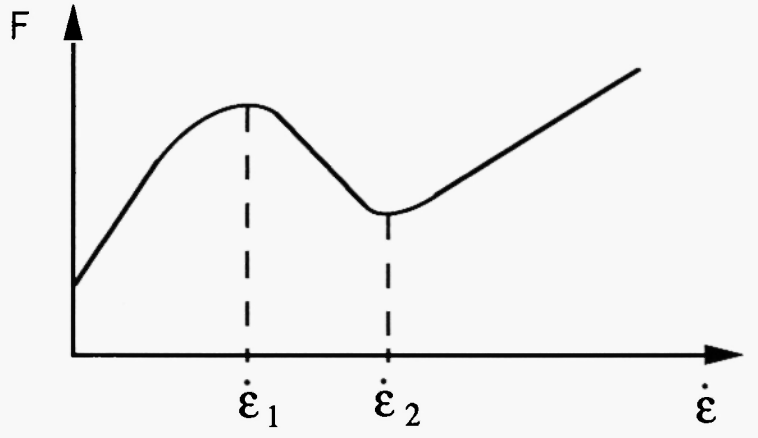

(b) Thermal component of stress F as a function of plastic strain rate $\dot{\epsilon}$. In the interval $(\dot{\epsilon}_1, \dot{\epsilon}_2)$, negative SRS is exhibited.

the f vs. v curve though it is somewhat distorted owing to the contribution of σ_d^{th} to the fact that the mobile dislocation density ρ_m entering the Orowan relation

$$\dot{\epsilon} = \phi \rho_m b v \tag{4}$$

between the plastic strain rate and the individual dislocation velocity is generally strain rate dependent. (Here b is the magnitude of the Burgers vector of mobile dislocations and ϕ is a geometric factor.)

2.2 Determining the intrinsic SRS

The constitutive equation (2) can be viewed as a result of integration of a general differential form

$$d\sigma = h d\epsilon + S d\ln\dot{\epsilon} \tag{5}$$

where the strain hardening rate $h = (\partial\sigma/\partial\epsilon)|_{\dot{\epsilon}}$ and the SRS $S = (\partial\sigma/\partial\ln\dot{\epsilon})|_{\epsilon}$ have been introduced. Indeed, eq. (5) is trivially integrable if h does not depend on $\dot{\epsilon}$ and S does not depend on ϵ. The fulfillment of the first condition will be simply assumed, while the second one is satisfied if S is identified with the corresponding derivative of F:

$$S = dF/d\ln\dot{\epsilon} \tag{6}$$

Equation (6) defines the intrinsic strain rate sensitivity of the flow stress following from the local constitutive behaviour. For uniform deformation, it coincides with the global, macroscopically measurable behaviour. In the case of nonuniform deformation associated with negative intrinsic SRS (see Section 3), the measurable, apparent SRS is not identical with the intrinsic one [12], as will be shown below.

In the early works [18,19], and later in [20–22], the qualitative shape of the curve shown on Fig. 3b has been recognized as a key property of DSA giving rise to the PLC effect. The macroscopic model due to Penning [23] is consistent with the microscopic considerations of Cottrell [14] and Friedel [15] and the mentioned refinements [16,17]

taking into account a jerky character of dislocation motion. In Penning's model [23] the term σ_d^a is replaced by $h\epsilon$. The deficiencies of Penning's model are obvious. Separation of the variables ϵ and $\dot{\epsilon}$ in two additive terms is definitely an approximation. The model is further limited by the assumption of constancy of h. Most serious is the fact that the plastic strain ϵ plays a role of a state variable which is only valid for materials with no strain path memory. However, these limitations are not too serious as long as small strains are considered which is the case when one band of localized deformation is passing. Despite the mentioned deficiences, Penning's model does capture the most significant features of the PLC effect, and it was adopted by the present authors [11,24,25]. It should be emphasized that in terms of eq. (1), the DSA effects enter through the friction component of stress, f. In an alternative approach by Kocks et al. [26–29], it is assumed that DSA comes about primarily via the effect of solutes on the dislocation junction strength. The model exploits the idea due to Sleeswijk [20] that solute redistribution near dislocation junctions, occurring by core diffusion, increases the glide resistance from the forest and that the effect becomes larger with increasing waiting time. The pertinent term in eq. (1) is, in this "dislocation model", σ_d.

2.3 Analytical form of intrinsic SRS

In accordance with eq. (3), the SRS given by eq. (6) is expressed as a sum of two terms

$$S = S_o + S_{ageing} \tag{7}$$

where

$$S_o = (\partial \sigma_d^{th} / \partial \ln \dot{\epsilon})|_\epsilon = kT/\gamma \tag{8}$$

stems from thermally activated breakaway of dislocations from localized obstacles in the absence of DSA and

$$S_{ageing} = df/d\ln\dot{\epsilon} \tag{9}$$

is associated with the strain rate dependence of the friction stress. In eq. (8) k is the Boltzmann constant and γ is the activation volume which characterizes thermally activated overcoming of localized obstacles.

For the discussion to follow, it is convenient to introduce t_w, the waiting time at a localized obstacle. Assuming that the average spacing between localized obstacles, ℓ, is proportional to the average spacing between forest dislocations, $\rho_f^{-1/2}$, and considering the free–flight time between the obstacles as negligible, one has

$$v = \ell/t_w \sim (\rho_f^{1/2} t_w)^{-1} \tag{10}$$

and

$$\dot{\epsilon} = \Omega/t_w. \tag{11}$$

Equation (11) is obtained from eq. (4) by substituting eq. (10) and introducing the elementary incremental strain

$$\Omega = \phi b \rho_m \rho_f^{-1/2}. \tag{12}$$

This is essentially a strain dependent quantity which corresponds to the deformation obtained when an elementary activation step is accomplished by all mobile dislocations. The ageing component of the SRS given by eq. (9) can be expressed as

$$S_{ageing} = - df/dlnt_w. \tag{13}$$

Equations (11) through (13) reflect two most important aspects of the Portevin–Le Châtelier effect mentioned in the Introduction. The dynamic interaction between mobile dislocations and solute atoms (i) is described by the function $f(t_w)$, while the collective

dislocation effects (ii) enter through the dislocation densities ρ_m and ρ_f evolving with strain. A complete description of the system is furnished by specifying the function $f(t_w)$ and the evolution equations for the two disloction densities.

First, we consider the dependence of f on the waiting time t_w. Taking f to be proportional to the solute concentration C_s at an arrested dislocation after a time $t = t_w$ and assuming the Cottrell–Bilby ageing kinetics [30] the solute concentration is expressed as

$$C_s = C_0(KDt_w)^{2/3} \tag{14}$$

where C_0 is the solute concentration in the bulk, far from the arrested dislocations ($C_s >> C_0$), D is the solute diffusivity and K is a constant which includes the solute–dislocation binding energy. Saturation effects at long ageing times can be accounted for by using a heuristic form of t_w–dependence of C_s [31]:

$$C_s = C_m\{1 - \exp[-\frac{C_0}{C_m}(KDt_w)^{2/3}]\} \tag{15}$$

where C_m is the saturation value of C_s. At small t_w, the Cottrell–Bilby relation (14) is recovered. Equation (15) leads to the following expression for f:

$$f = f_0\,[1 - \exp -(t_w/\tau_0)^{2/3}]. \tag{16}$$

Here the saturation value f_0 represents the maximum increase in stress associated with DSA; the characteristic time τ_0 reads

$$\tau_0 = (KD)^{-1}(C_m/C_0)^{3/2} \tag{17}$$

This quantity contains information on the kind of diffusion process underlying DSA.

Second, the collective dislocation behaviour affects the PLC effect through the elementary incremental strain $\Omega = \phi b \rho_m \rho_f^{-1/2}$. Indeed, at a given strain rate, the evolution of Ω with strain influences the waiting time, cf. eq. (11). This imposes an indirect strain dependence of the friction stress f and, consequently, of the ageing component S_{ageing} of the SRS. This fact makes it possible to explain the experimental finding that DSA effects are strain dependent. To account for this dependence, it was assumed in a number of studies, e.g. [16,17,32], that the mobile dislocation density increases with strain and that the diffusivity D in substitutional solid solutions grows with ϵ, too. The latter depencence was ascribed in the mentioned works to the increase with deformation of vacancy concentration entering as a factor in the substitutional solute diffusivity.

To investigate the strain dependence of Ω, coupled evolutionary differential equations for ρ_m and ρ_f have to be formulated. A corresponding model has been proposed in Ref. 33. Without going into detail here, we just mention that at small plastic strains the mobile dislocation density increases with strain faster than the forest density, while at large strains, the density of forest dislocations increases faster, the mobile density being close to saturation [34]. Thus, Ω increases at small strains from an initial value Ω_o, passes through a maximum and decreases with strain (nearly as the ivnerse of σ_d), asymptotically approaching a saturation value Ω_s [33,34] (see Figure 8 below).

The intrinsic strain rate sensitivity can be conveniently represented in the nondimensional form. Combining eqs. (7), (9) and (16) yields

$$s = s_o - X\exp(-X) \tag{18}$$

where

$$s = (3/2)(S/f_0), \quad s_0 = (3/2)(S_0/f_0) \tag{19}$$

and

$$X = (t_w/\tau_0)^{2/3} = (\Omega/Z)^{2/3}. \tag{20}$$

Here the quantity $Z = \dot{\epsilon}\tau_0$ has been introduced which bears some similarity with the Zener–Hollomon parameter often used in studies on creep. It is recognized that the effect of strain rate and temperature enters the DSA–related term $-X\exp(-X)$ through this parameter. (Note that the characteristic time τ_0 is associated with solute diffusivity (cf. eq. (17)) and is given by an Arrhenius–type formula.) The nominal solute concentration C_0 is contained in this parameter as well. Finally, as already mentioned, a strain dependence is incorporated through the elementary incremental strain Ω. The SRS in the absence of DSA, S_0 (and, consequently, the corresponding dimensionless quantity s_0) is proportional to σ_d in materials which exhibit the so called Cottrell–Stokes behaviour, e.g. in fcc metals, and is practically constant in bcc metals. For the sake of simplicity, a "model material" with a constant s_0 will be considered below.

It is readily recognized from eq. (18) that s can only be negative if s_0 is smaller than the maximum value, 1/e, of the bell–shaped function $X\exp(-X)$. In such a case, as will be illustrated below, there is a range of X, i.e. of strain rates and temperatures, within which the SRS, s, is negative.

3. The instability mechanism

3.1 Linear stability analysis and instability criterion

The essence of the instability mechanism leading to jerky flow and nonuniform deformation is easily rationalized by investigating the stability of uniform flow in a material obeying Penning's constitutive equation. As shown in [35], the result obtained is,

however, quite general. The imposed external condition is that of constant stress rate: $\dot{\sigma} = \dot{\sigma}_0 =$ const leading to

$$\dot{\sigma}_0 t = h\epsilon + F(\dot{\epsilon}) \tag{21}$$

This equation has a uniform steady state solution $\dot{\epsilon} = \dot{\epsilon}_s = \dot{\sigma}_0/h =$ const. The same uniform steady state can equivalently be reached by straining with a constant plastic strain rate $\dot{\sigma}_0/h$. By differentiating eq. (21) with respect to time one obtains

$$\ddot{\epsilon} = -\frac{h}{dF/d\dot{\epsilon}}(\dot{\epsilon} - \dot{\epsilon}_s) \tag{22}$$

Linearizing eq. (22) around its steady state value, small local deviations from steady state can be introduced in the form $\delta\dot{\epsilon} = \dot{\epsilon} - \dot{\epsilon}_s = (\delta\dot{\epsilon})_0 \exp(\lambda t), \delta\ddot{\epsilon} = \lambda\delta\dot{\epsilon}$, where $(\delta\dot{\epsilon})_0$ is a constant and time t is reckoned from the moment the perturbation has been introduced. Inserting into eq. (22), we obtain the growth parameter (bifurcation coefficient) λ:

$$\lambda = -h/(dF/d\dot{\epsilon})|_{\dot{\epsilon}=\dot{\epsilon}_s} = -h\dot{\epsilon}/S(\dot{\epsilon}_s). \tag{23}$$

A positive λ indicates a growing localization. Bifurcation from uniform to nonuniform deformation occurs at the point where λ changes sign. In the case under consideration λ becomes positive when the SRS, S, turns negative. It follows that the domain of the occurrence of the PLC effect is defined by the condition that the loading rate or the strain rate at steady state are such that $S(\dot{\epsilon}_s) < 0$.

Experimentally, the apparent SRS, as measured through strain rate jump tests, may already be slightly negative when jerky flow begins [26]. A modified localization condition accounting for this fact was proposed recently by McCormick [13] who con-

sidered the kinetics of transition of solute concentration to its new quasi–steady state value. In what follows, the condition $s = 0$ will be still considered as a "demarkation line" between stable and unstable deformation, however.

3.2 Temporal behaviour

The evolution of the plastic strain rate $\dot{\epsilon}$ in a given cross–section can be investigated by considering its time derivative given by eq. (22). The sign of this derivative depends on the location of the point $\dot{\epsilon} = \dot{\epsilon}_s$ with respect to the interval $(\dot{\epsilon}_1, \dot{\epsilon}_2)$ where $dF/d\dot{\epsilon}$ is negative (Figs. 3b and 4). For $\dot{\epsilon}_s < \dot{\epsilon}_1$, $dF/d\epsilon$ is positive and any deviation of $\dot{\epsilon}$ from the steady state value will decrease with time. Uniform steady state is thus stable, in accord with the result of linear stability analysis.

Consider now the case when $\dot{\epsilon}_s$ falls within the interval $(\dot{\epsilon}_1, \dot{\epsilon}_2)$:

$$\dot{\epsilon}_1 < \dot{\epsilon} < \dot{\epsilon}_2 \tag{24}$$

Starting with $\dot{\epsilon} = 0$, the strain rate will grow, $\ddot{\epsilon}$ being positive. This growth will go on

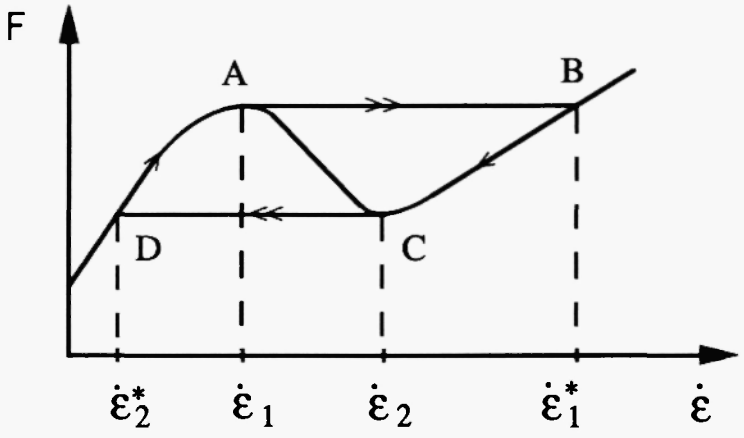

Fig. 4. Relaxation oscillations behaviour consisting in strain rate jumps A→C and B→D and continuous variation of $\dot{\epsilon}$ along the ascending branches, DA and CB, of the $F(\dot{\epsilon})$ characteristic.

until $\dot{\epsilon}$ will reach the value $\dot{\epsilon}_1$ at which point $dF/d\dot{\epsilon}$ vanishes and $\ddot{\epsilon}$ becomes infinite, cf. eq. (22). The strain rate is then bound to change instantaneously, and a jump to $\dot{\epsilon} = \dot{\epsilon}_1^*$ will take place (Fig. 4). The system will thus find itself on the opposite ascending branch of the F vs. $\dot{\epsilon}$ curve. Here, again, $dF/d\dot{\epsilon} > 0$ so that $\ddot{\epsilon}$ is negative. The plastic strain rate will decrease tending again to the steady state value. On reaching the point $\dot{\epsilon} = \dot{\epsilon}_2$, $\ddot{\epsilon}$ turns infinite again, and another jump, now to $\dot{\epsilon} = \dot{\epsilon}_2^*$, will occur. A continuous increase of $\dot{\epsilon}$ will resume, until the point $\dot{\epsilon} = \dot{\epsilon}_1$ will be reached and the jump $\dot{\epsilon}_1 \rightarrow \dot{\epsilon}_1^*$ will be repeated. This succession of events in which continuous variation of plastic strain rate along the branches DA and CB is interrupted by strain rate jumps (A → C and B → D) onto the opposite ascending branch of the $F(\dot{\epsilon})$ characteristic will recur periodically. The system permanently tends to the steady state value lying in the "forbidden gap" $(\dot{\epsilon}_1, \dot{\epsilon}_2)$, but can never enter this strain rate interval. In other words, when forced by the imposed loading conditions to deform with $\dot{\epsilon}_s$ from within the forbidden gap, the material in an individaul cross–section spends one part of a period in the range of small strain rates (DA), where mobile dislocations drag along their solute atmospheres, and the other in the range of large strain rates (CB), where mobile dislocations are free from solute clouds. The jumps A → C and B → D correspond to depinning and pinning of mobile dislocations, respectively. The temporal behaviour along the low and high velocity branches can easily be estimated [11] by integrating eq. (22), provided the shape of the $F(\dot{\epsilon})$ curve is known in the ranges where its slope is positive:

$$-\mathrm{ht} = \int \frac{\mathrm{d}F(\dot{\epsilon})}{\mathrm{d}\dot{\epsilon}} \cdot \frac{\mathrm{d}\dot{\epsilon}}{\dot{\epsilon} - \dot{\epsilon}_s} \tag{25}$$

After one cycle of temporal oscillations one has $\Delta F = 0$, and from Penning's equation, eq. (23), the plastic strain increment $\Delta\epsilon$ and the time period ΔT are such that $\dot{\sigma}_o/h = \dot{\epsilon}_s = \Delta\epsilon/\Delta T$.

The average over the period in a given cross–section is maintained at the prescribed value $\dot{\epsilon}_s$. The average over the entire gauge length can be kept if parts of the specimen deform with the strain rates corresponding to range DA and parts to range BC. Stratification of the deforming material into bands is thus inherent to this deformation regime.

The temporal variation of the plastic strain rate in an individual cross–section following the periodic pattern described is shown in Fig. 5. The cycles of slow–fast–slow–fast variation of $\dot{\epsilon}$ are referred to as relaxation oscillations [36,25]. The class of nonlinear phenomena related to relaxation oscillations is encountered quite frequently. Common to the systems of this class is a negative characteristic analogous to negtive SRS in case of the PLC effect. As an example closely related to the PLC effect, the Gunn effect should be mentioned [37]. It is observed in bulk semiconductors exhibiting a range of negative differential resistivity. Another example is pull–out of a metallic filament from a polymeric matrix where the relevant characteristic is a negative friction coefficient for low

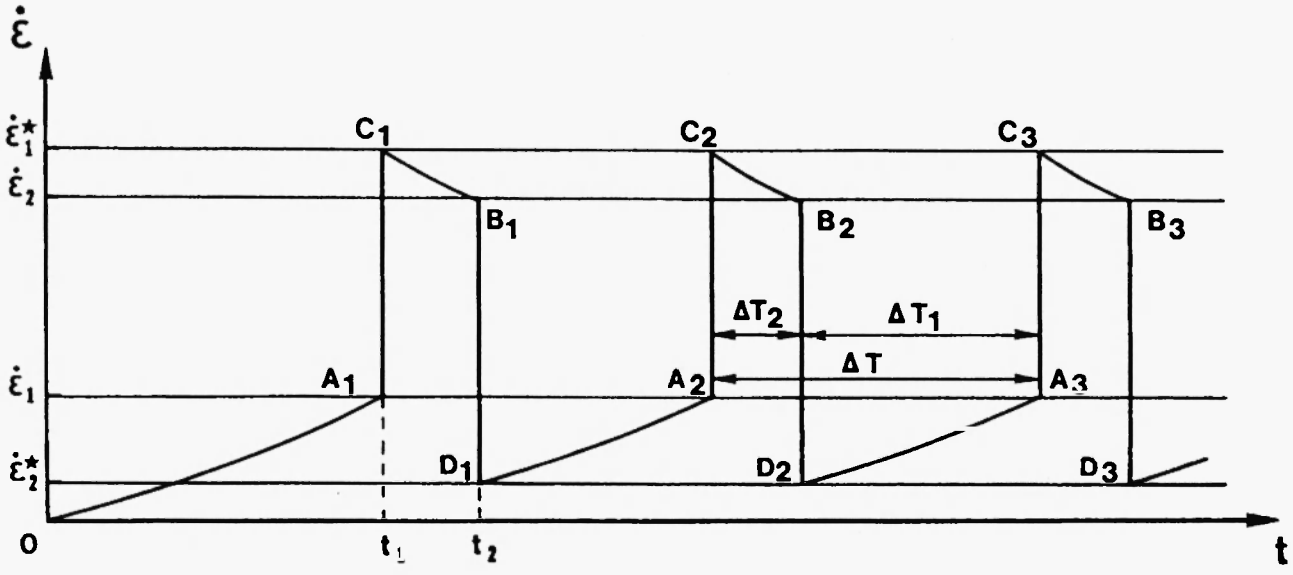

Fig. 5. Strain rate profile as a function of time at a given location within a specimen. Strain rate jumps A→C and B→D (Fig. 4) are found again in this diagram as the jumps $A_i \rightarrow C_i$ and $B_i \rightarrow D_i$, respectively.

displacement velocities [38]. Further examples have been discussed in Refs. 25 and 39. A translation of the results appears rather straightforward.

3.3 Spatial aspects

Turning back to the PLC effect we should stress the spatial aspects. The constitutive equation (21) underlying the present analysis does not contain a spatial coordinate. If all parts of a specimen could deform coherently, in "phase", the global behaviour would coincide with the local behaviour characterized by relaxation oscillations of the plastic strain rate. Such a coherency is not possible for usual specimen lengths, so that the temporal pattern discussed above should propagate along the gauge length. Indeed, it can easily be demonstrated [24,25] that the constitutive description used admits of solutions propagating with an arbitary constant velocity V. The strain rate profile along the specimen axis, taken at a fixed time, exhibits a band–like shape (Fig. 6). The regions of increased plastic strain rate (B_1C_1, B_2C_2, B_3C_3, etc...) can be referred to as the PLC bands. A remarkable feature of these deformation bands is that they have sharp edges on

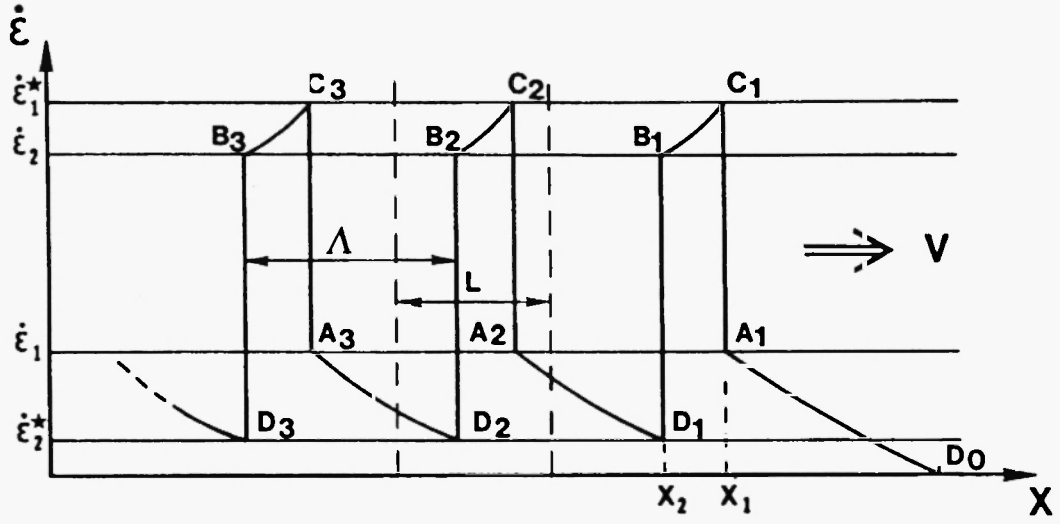

Fig. 6. Strain rate profile as a function of coordinate at a fixed time. The spatial period Λ is related to the time period ΔT, cf. Fig. 5, via the pattern propagation velocity V according to eq. (26). The specimen gauge length is denoted by L.

both sides. This spatial pattern propagating at a velocity V is a reflection of the temporal pattern at a given specimen cross–section (Fig. 5). The spatial period Λ is related to the temporal period ΔT via

$$\Lambda = V\Delta T. \tag{26}$$

Similarly, the band width, w, is related to the duration ΔT_2 of the continuous decrease of strain rate from $\dot{\epsilon}_1^*$ to $\dot{\epsilon}_2$ via

$$w = V\Delta T_2. \tag{27}$$

The passage of each PLC band across the gauge length is recorded in a stress–strain curve as a steep strain increment, whereas the strain increment associated with slow deformation between the bands is incomparably smaller. A typical stair–case deformation curve is produced as illustrated in Fig. 7 by a strain vs. stress curve for Al–5%Mg deformed with a constant stress rate of 0.1 MPa/s at room temperature [40]. The above

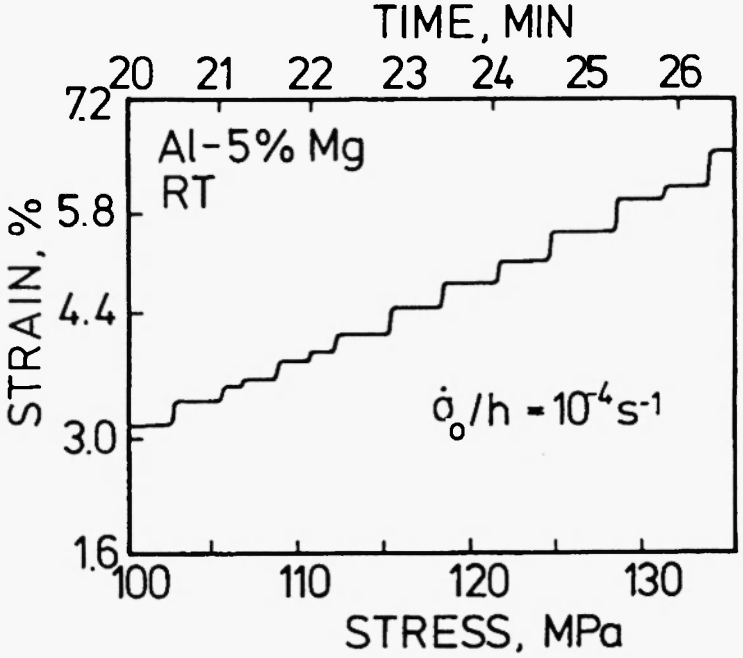

Fig. 7. A stair–case deformation curve of Al–5%Mg deformed with a constant stress rate in the PLC regime (after [40]).

considerations imply that the shape of the stress vs. stress diagram determined by the loop ACBD is independent of the magnitude of $\dot{\sigma}_o$, provided that $\dot{\epsilon}_s = \dot{\sigma}_o/h$ lies anywhere in the interval $(\dot{\epsilon}_1, \dot{\epsilon}_2)$. This conclusion contradicts the experimental observation that the magnitude of the strain bursts or stress drops decreases with increasing stress rate or strain rate [41,42]. The contradiction is removed [43] by taking into account the variation of the thermal component of stress during a waiting time. The intrinsic SRS is then modified in such a way that the shape of the $F(\dot{\epsilon})$ characteristic explicitly depends on $\dot{\sigma}_o$. These stress rate effects are illustrated in Sec. 4.2, while a detailed presentation of modelling them is given in Ref. 43. Here we would only like to emphasize a parallel between two modes of straining: with constant stress rate and constant strain rate. The first one, considered here, is much easier to treat [11] because, under these conditions, the stress remains constant during the propagation of a deformation band, and the propagation occurs with constant velocity. The mathematical description of the temporal variation of the mechanical quantities (plastic strain, plastic strain rate and stress) in a given material cross–section is especially easy in the case of $\dot{\sigma} =$ const.

The conditions for the occurrence of the PLC effect under constant imposed strain rate, $\dot{\epsilon}_a$, can be inferred from the corresponding conditions for constant stress rate testing [25]. The strain rate interval in which the PLC effect occurs in the former case is given by

$$\frac{h+M}{hM}\dot{\sigma}_{o1} < \dot{\epsilon}_a < \frac{h+M}{hM}\dot{\sigma}_{o2} \qquad (28)$$

where $(\dot{\sigma}_{o1}, \dot{\sigma}_{o2})$ is the interval of stress rates corresponding to the occurrence of the PLC effect under constant stress rate testing. M denotes the combined elastic modulus of specimen and testing machine.

During a discontinuity of plastic flow ("jerk"), there is generally a drop in stress,

$\Delta\sigma$ ($\Delta\sigma<0$), and a strain burst, $\Delta\epsilon$. By taking the difference of the values of stress and strain between points C and B of the characteristic curve $F(\dot{\epsilon})$, cf. Fig. 4, we have:

$$\Delta\sigma = h\Delta\epsilon + \Delta F \tag{29}$$

where $\Delta F = F(C)-F(B)$ is the difference between the maximum and the minimum value of the characteristic curve which can be considered as an intrinsic amplitude of the PLC effect for the material considered. During a short time interval of a jerk, the stiffness of the tensile system comes into play through the relation $\Delta\sigma + M\,\Delta\epsilon \approx 0$, which, combined with eq. (29), yields the amplitude of the load drops and the strain bursts:

$$\Delta\epsilon = -\Delta\sigma/M = -\Delta F/(h+M)\,. \tag{30}$$

It follows that a hard tensile system ($h<<M$) will translate the PLC instabilities into load drops of amplitude $\Delta\sigma \approx \Delta F$, while in a soft tensile system ($h>>M$) and under constant stress rate ($M = 0$) one will mainly observe strain bursts of amplitude $\Delta\epsilon \approx -\Delta F/h$. As mentioned above, the intrinsic amplitude ΔF depends in practice on the applied stress rate, or on the equivalent applied strain rate $\dot{\sigma}_c/h$. As a consequence, the recorded amplitudes of strain bursts or load drops, which are both proportional to ΔF, will have the same dependence on the applied rate whatever the mode of testing and the stiffness of the tensile system.

Concluding this section we would like to stress that any experimental determination of the SRS in the region where it is negative can only yield an apparent quantity. The intrinsic SRS remains hidden by its very nature, for strain rates from within the forbidden gap cannot be attained physically. On the other hand, the exact shape of the $F(\dot{\epsilon})$ characteristic in the forbidden gap is of no relevance for a description of the PLC

effect [24]. However, the knowledge of the exact position of the extrema of the curve and its shape in proximity to them in the range of positive slope is extremely important for theory.

4. Macroscopic features of PLC instabilities

The above considerations make it possible to discuss macroscopic manifestations of the PLC effect on the basis of the model integrating DSA effects with collective dislocation behaviour and effects of the applied stress rate or strain rate.

4.1 The critical strains

We proceed from the condition

$$S \leq 0 \tag{31}$$

which, with some limitations mentioned in Sect. 3, provides a criterion for the occurrence of the PLC effect. For solutions to exist, s_0 must be smaller than 1/e, cf. Sect. 2. When this is the case, there are two solutions, $X_1 < 1$ and $X_2 > 1$, of eq. (18) which expresses the critical condition for the onset of PLC instabilities. Accordingly, for given strain rate and temperature, this defines two critical values, $\Omega_1 = ZX_1^{2/3}$ and $\Omega_2 = ZX_2^{2/3}$, of the elementary incremental strain (cf. eq.(20)).

The PLC domain can now be easily determined by placing a strip limited by the horizontal lines $\Omega = \Omega_1$ and $\Omega = \Omega_2$ onto the Ω vs. ϵ diagram of Fig. 8 and by determinign the intersections. A wealth of various possibilities opens, depending on the values of the plastic strain rate, temperature, and the nominal solute concentration C_0 which determine the location of the strip with respect to the $\Omega(\epsilon)$–curve. Variation of one of these parameters leads to a displacement of the strip along the Ω–axis accompanied by variation of the band width.

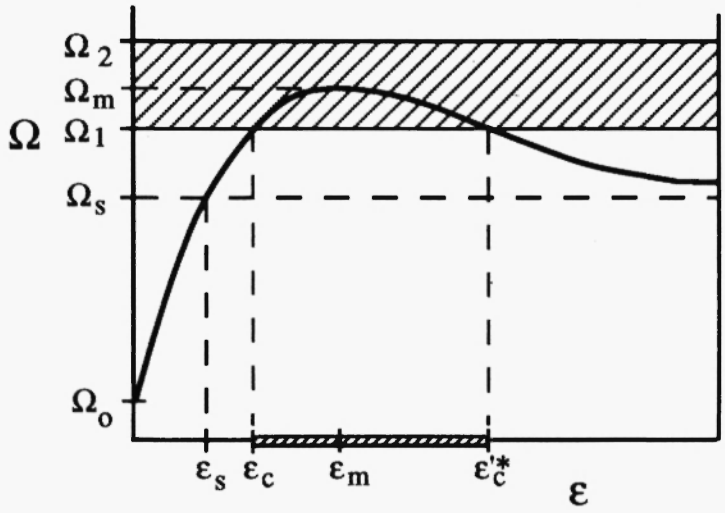

Fig. 8. Elementary incremental strain Ω as a function of ϵ. Ω_0, Ω_m, and Ω_s denote the initial, the maximum, and the saturation values, respectively. The negative SRS range (i.e. the PLC domain) is represented by the hatched strip bounded by the horizontal lines $\Omega = \Omega_1$ and $\Omega = \Omega_2$. The lower (ϵ_c) and upper ($\epsilon_c'^*$) critical strains are shown.

Consider an example shown in Fig. 8. The bottom line of the band, $\Omega = \Omega_1$, intersects the $\Omega(\epsilon)$ profile twice, at $\epsilon = \epsilon_c$ and $\epsilon = \epsilon_c'^*$. Jerkey flow will occur in this interval. Under real deformation conditions, $\epsilon_c'^*$ may be too large to be recorded so that the upper critical strain is not systematically observed. An example, found on an Al–Li alloy at 300K (unpublished work), is shown in Fig. 9a.

Obviously, no PLC effect will occur if the strip is located below the Ω vs. ϵ profile, i.e. $\Omega_2 < \Omega_0$ (cf. Fig. 8). This corresponds to sufficiently low strain rates and/or high temperatures. Likewise, there will be no PLC effect for $\Omega_1 > \Omega_m$ (where Ω_m is the maximum value of Ω) for which case the strip is located above the elementary incremental strain profile. This corresponds to sufficiently high strain rates and/or low temperatures. The threshold conditions for the occurrence of the PLC effect are thus $\Omega_1 = \Omega_m$ and $\Omega_2 = \Omega_0$. Expressing the above conditions in terms of $\dot{\epsilon}$, a PLC domain is obtained:

$$\Omega_0/(\tau_0 X_2^{3/2}) < \dot{\epsilon} < \Omega_m/(\tau_0 X_1^{3/2}). \tag{32}$$

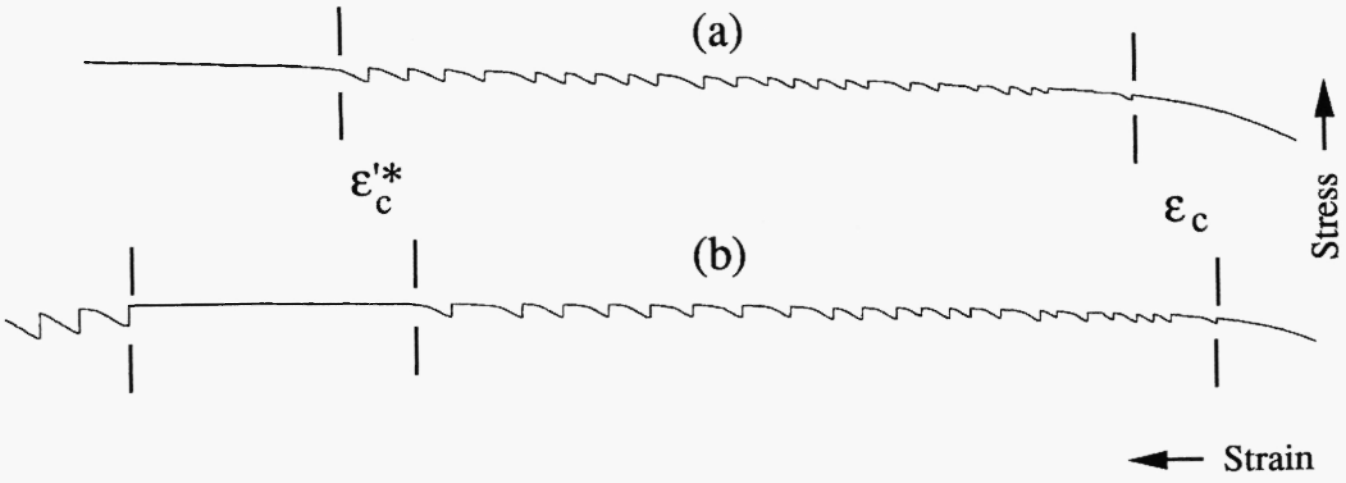

Fig. 9. Time dependence of stress in an Al–Li alloy deformed at room temperature with a constant strain rate.
(a) A curve exhibiting a lower and an upper critical strain ($\dot{\epsilon} = 1.75 \cdot 10^{-5}$ s^{-1}).
(b) A curve showing two regions of jerky flow separated by a smooth region ($\dot{\epsilon} = 2 \cdot 10^{-5}$ s^{-1}).

A sufficient condition for the occurrence of the PLC effect is therefore the fulfillment of inequalities (32). Otherwise, DSA simply results in a decrease of the SRS which, however, remains positive and does not give rise to PLC instabilities. With typical numerical values for Al–5%Mg and with the value $\tau_0 = 1s$ for the characteristic time associated with diffusion, i.e. typically around room temperature, inequalities (32) read $1.8 \cdot 10^{-6} s^{-1} < \dot{\epsilon} < 5.8 \cdot 10^{-2} s^{-1}$ [33]. This compares reasonably well with the experimental range of existence of the PLC effect.

Various possibilities with regard to the number and position of the critical strains for the occurrence of jerky flow have been analysed in Ref. 33. The strain rate dependence of the critical strains can be investigated by tracing the variation of width and position of the strip bounded by the horizontal lines $\Omega = \Omega_1$ and $\Omega = \Omega_2$. One of four most representative dependences is illustrated by Fig. 10 where the positions of the PLC intervals

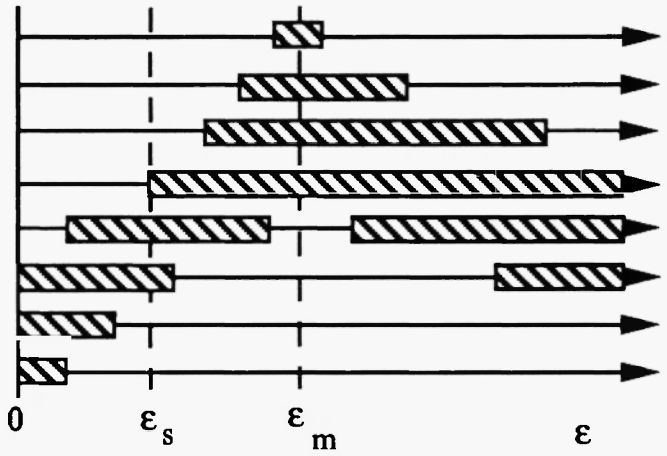

Fig. 10. One of four most likely sequences of diagrams illustrating the strain rate dependence of the critical strains. Strain rate increases (or, equivalently, temperature decreases) from bottom to top. The regions of jerky flow are hatched.

(hatched regions) are shown as a function of strain rate at a fixed temperature or, alternatively, as a function of temperature for a given strain rate. From this figure, one can see how the number and position of the critical strains change depending on deformation conditions. While no observation of all four critical strains on a single stress–strain curve is available to our knowledge, such striking feature of the described behaviour as merging of intervals of jerky flow with increasing strain rate of decreasing temperature has been observed by Räuchle et al. [44] on Cu–3.3 at% Sn. This is illustrated by Fig. 11. The existence of two regions of jerky flow separated by a smooth portion of deformation curve was found on Al–Li (unpublished work), Fig. 9b.

The strain rate dependence of the critical strain, ϵ_c, at which the PLC effect first sets in, is of particular interest. For most alloy systems exhibiting the PLC effect, ϵ_c increases with strain rate, cf. e.g. [32]. A plot of log $\dot{\epsilon}$ vs. log ϵ_c yields a straight line with a slope ranging from 2 to 3 for substitutional and from 0.5 to 1 for interstitial alloys. The difference in this exponent between substitutional and interstitial solutes is explained by a number of authors [16,17] by the above mentioned assumption of accumulation with strain

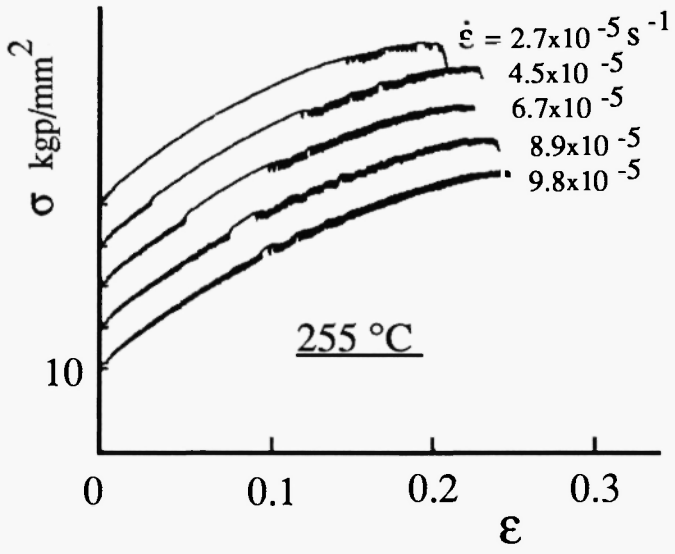

Fig. 11. A stress–strain curve with two regions of jerky flow separated by a smooth region in a Cu–3.3at%Sn alloy at 255°C (after Räuchle et al. [44]).

of deformation–induced vacancies whose concentration enters the diffusivity of substitutional solutes, but does not affect that of interstitial ones. There is no consensus on the origin of this difference among researchers, though, cf. Ref. 28.

The model outlined above yields a strain rate dependence of ϵ_c which can be roughly approximated by a power law [33]. The exponent obtained (0.5 to 1) stems from the evolution with strain of the dislocation densities ρ_m and ρ_f (primarily ρ_m) and does not take into account any possible strain dependencies of solute diffusivity. It compares fairly well with the $\dot{\epsilon}$ dependence of ϵ_c measured on interstitial alloys [33].

An interesting feature, observed in Al based substitutional solid solutions [45–48,9] and in carbon steels [49,50], is that at low strain rates and high temperatures an "inverse" behaviour is found: the critical strain increases with decreasing strain rate and increasing temperature. The ranges of "normal" and "inverse" behaviour in a corresponding log ϵ_c vs. log $\dot{\epsilon}$ curve are thus separated by a minimum. The mechanism by which the critical

strain is affected is not clearly understood at present, although there is some evidence that it is linked to precipitation before or during the deformation test [9].

4.2 The rate dependence of jerky flow

Now, after we dwelt on the conditions for the occurrence of the PLC effect, we turn to a description of its observable features. First, characteristic features of deformation curves, such as stress drops under constant strain rate loading and strain bursts under constant stress rate loading, will be considered. Then, the characteristics of the associated deformation bands will be described (Sect. 4.3).

Repeated stress drops, of the type depicted on Fig. 1, are recorded in a hard testing machine during deformation with constant imposed strain rate, $\dot{\epsilon}_a = \text{const}$. A staircase curve of the kind of Fig. 7 is a typical diagram for constant stress rate deformation. As mentioned in Sect. 3.3 (cf. also eq. (30)), the amplitude of stress drops or strain bursts is determined in the first case by the difference ΔF of the maximum and the minimum values of the corresponding dynamic, i.e. rate dependent, characteristic.

The static reference curve $F(\dot{\epsilon})$ as well as a family of dynamic curves $F(\dot{\epsilon},\dot{\sigma}_0)$ computed on the basis of the model [43] for various strain rates and at a constant strain value ($\Omega = 10^{-2}$, corresponding to a strain of a few percent) are depicted on Fig. 12 together with the strain rate jumps which accompany the relaxation oscillation behaviour. Typical parameter values for Al–5%Mg at room temperature have been used for these and the following numerical estimates. The range of stress rates ($\dot{\sigma}_{01}$, $\dot{\sigma}_{02}$) is such that inequalities [32] are fulfilled. The magnitude of ΔF, which is proportional to the amplitude of the PLC jerks, decreases with increasing applied stress (or strain) rate. This behaviour is rationalized by considering that, during the reloading sequence following a jerk there is a competition between ageing effects which tend to increase the waiting time and the

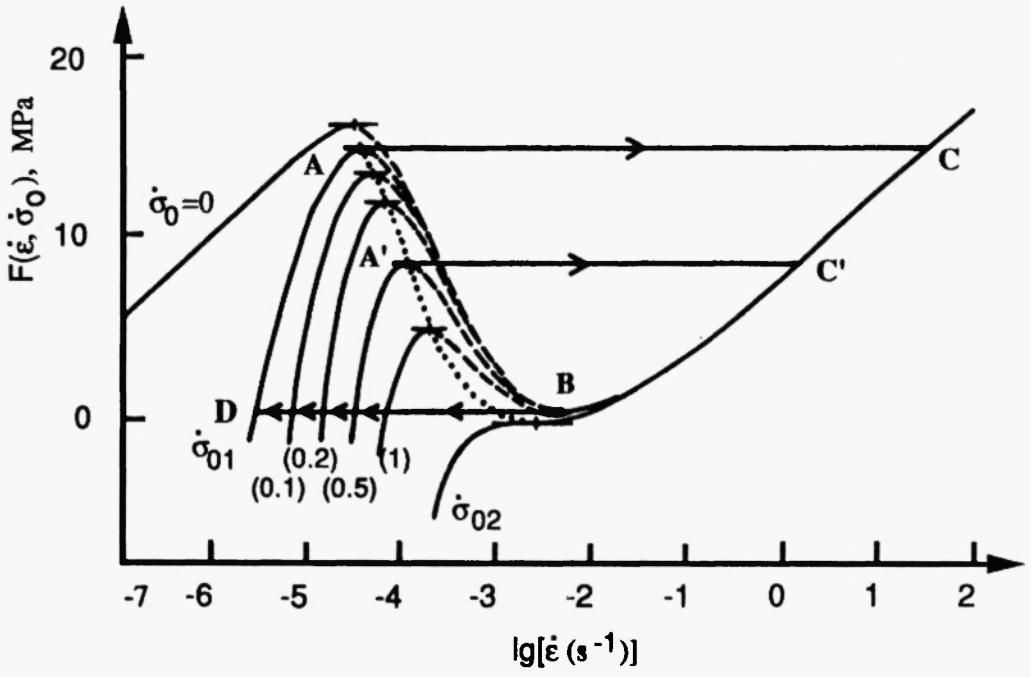

Fig. 12. Dynamic $F(\dot{\epsilon})$ characteristic showing a dependence on the imposed stress rate $\dot{\sigma}_0$ (indicated in the parentheses). The variation of the strain rate is described by cycles such as ABCD or A'B'C'D'. The dotted curve connects the critical points for the onset of PLC jumps at various $\dot{\sigma}_0$.

loading rate which tends to reduce it. Ageing effects are thus largest at low (stress) rates, and the magnitude of jerks decreases until it vanishes at the upper boundary of the PLC interval.

Turning to equivalent constant strain rate testing,it is interesting to note that the top value of a stress drop, which corresponds to the maximum of a particular $F(\dot{\epsilon})$ curve, decreases with $\dot{\epsilon}_a$, while the bottom value, associated with the minimum of the curve largely remains constant. The $\dot{\epsilon}_a$ dependence of the top stress in the forbidden gap $(\dot{\epsilon}_1, \dot{\epsilon}_2)$ qualitatively follows the descending branch of the reference (static) curve $F(\dot{\epsilon})$. Thus, by measuring this apparent SRS, the intrinsic SRS can be studied qualitatively. The apparent SRS for Al–5%Mg measured at room temperature in the described manner [25] is shown on Fig. 13 as a function of the applied stress rate. (Note that the term $h\epsilon$ has to be detracted from the stress for the function related to $F(\dot{\epsilon})$ to be obtained.) The positions of

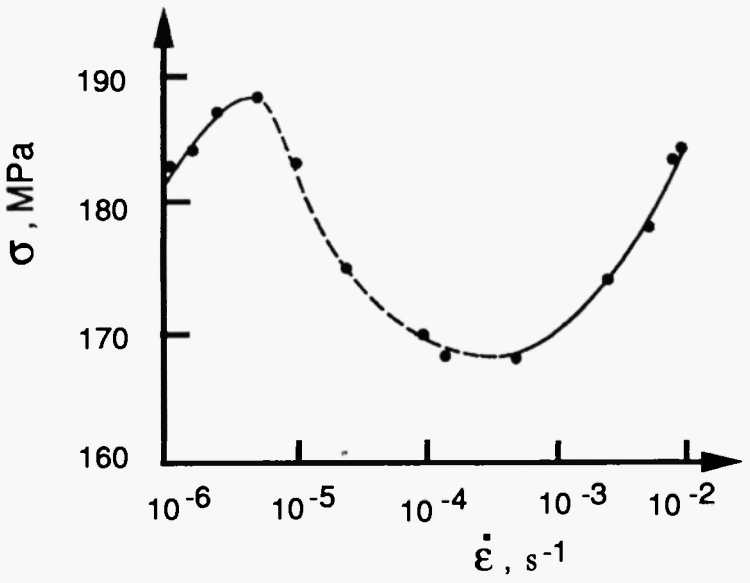

Fig. 13. Upper stress of PLC serrations at $\epsilon = 8\%$ as a function of imposed strain rate in Al–5%Mg at room temperature [25].

the extrema of this function provide a measure of the boundary values for the stress rate range of the PLC effect. Direct determination of the boundary values of strain rate indicates a satisfactory accuracy of this procedure [25].

To obtain an exact relation between, e.g. the strain burst amplitude, $\Delta\epsilon_b$, under constant stress rate loading and ΔF, the time ΔT_2 has to be calculated. The latter quantity is that portion of the relaxation oscillations period which corresponds to the high strain rate part (CB) of the trajectory ACBD in Fig. 4. Applied to the initial and the final states of a strain burst, the constitutive equation (21) yields

$$\dot{\sigma}_0 \Delta T_2 = h\Delta\epsilon_b + \Delta F. \tag{33}$$

The expression for ΔT_2 can be obtained from eq. (25), the integration being carried out from $\dot{\epsilon}_1^*$ to $\dot{\epsilon}_2$.

From eq. (33), the main contribution to $\Delta\epsilon_b$ arises from the term $\Delta F/h$ which decreases with increasing stress rate. The term $\dot{\sigma}_0 \Delta T_2$ increases with strain rate and may

become significant at large $\dot{\epsilon}$. However, in most of the PLC range $\Delta\epsilon_b$ is approximately equal to $\Delta F/h$. The stress drop amplitude in constant strain rate loading is accordingly given by ΔF. It is interesting to inquire about the strain dependence of $\Delta\epsilon_b$. Investigation of the strain dependence of the dynamic characteristic curves, entering through Ω, reveals that ΔF is rather insensitive to strain. The term $\dot{\sigma}_0\Delta T_2$ does depend on ϵ via Ω. Without going into detail we just mention that ΔT_2 decreases with increasing Ω. Consequently, when Ω increases, so does the strain burst amplitude. Since under usual conditions Ω increases with strain (though it may exhibit a maximum, cf. Fig. 8), the general tendency is an increase of $\Delta\epsilon_b$ with strain.

The experimental results obtained by Karimi [51] can be interpreted in favour of the model leading to the discussed dependences. The data obtained on an austenitic stainless steel in a soft machine are shown in two diagrams, as $\Delta\epsilon_b$ vs. $\dot{\sigma}_0$ plots taken at various strains (Fig. 14) and as $\Delta\epsilon_b$ vs. ϵ plots taken at a fixed stress rate for various

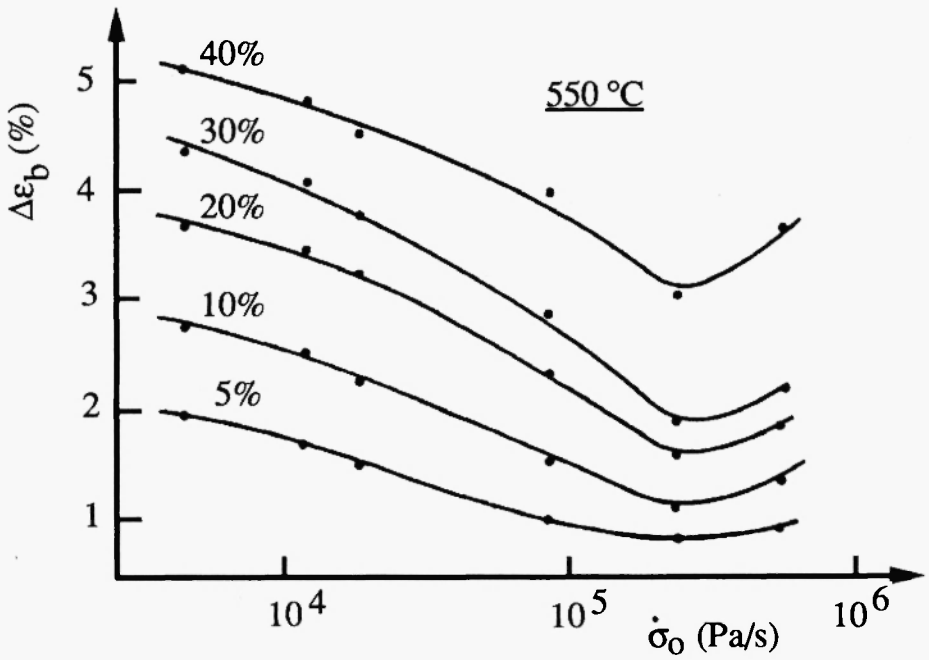

Fig. 14. Strain burst magnitude (plastic strain within a band) as a function of stress rate for various strains in an austenitic stainless steel. (After Karimi [51]).

temperatures (Fig. 15). It is recognized that even small details, such as a weak increase of $\Delta\epsilon_b$ at large stress rates (Fig. 14) are in accord with the above predictions of the model. Karimi [51] distinguishes three stages in the strain dependence of $\Delta\epsilon_b$ shown on Fig. 15 and mentions that stage III is associated with necking. It is evident then that stage I may be associated with the fast initial increase of Ω with strain while stage II may correspond to saturation behaviour of Ω at larger strains.

Also consistent with experiment is the behaviour with stress rate of the portion ΔT_1 of the period of relaxation oscillations. Defined as the time between strain bursts, it can also be associated with reloading time in constant strain rate testing. The computed dependence presented in Fig. 16 shows a fairly good agreement with a measured one (Fig. 17). It should be mentioned that the reloading time $\Delta T_1(\dot{\sigma}_0)$ is larger than the elastic reloading time, $\Delta F/\dot{\sigma}_0$, which indicates that there is some plasticity, up to 0.5 %, during reloading. This effect is especially pronounced at small stress rates.

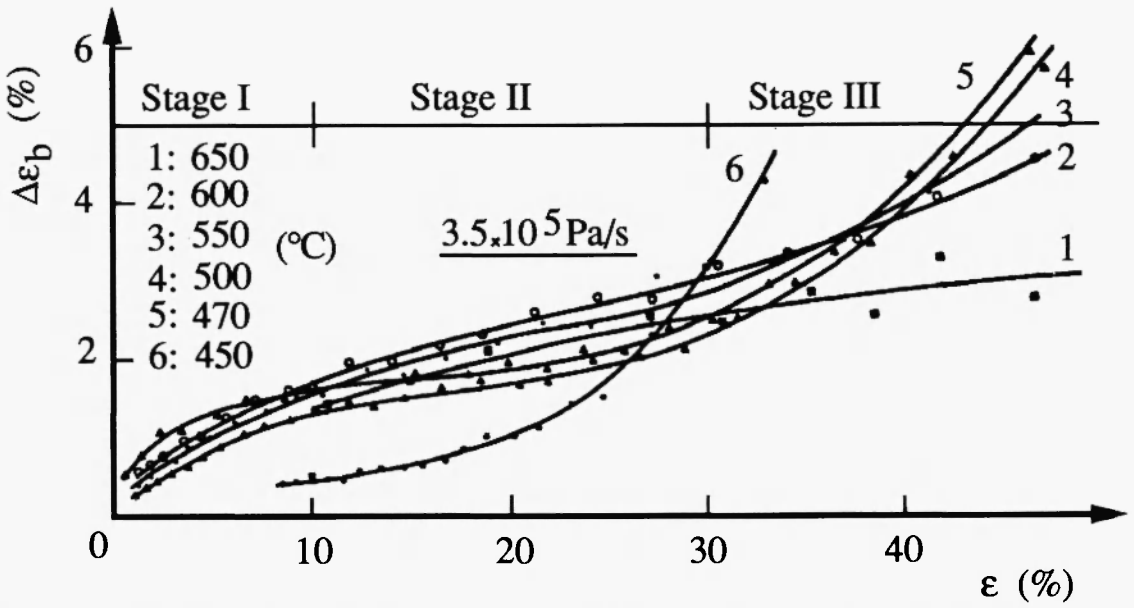

Fig. 15. Strain burst magnitude (plastic strain within a band) as a function of strain for a fixed stress rate and various temperatures in an austenitic stainless steel. (After Karimi [51]).

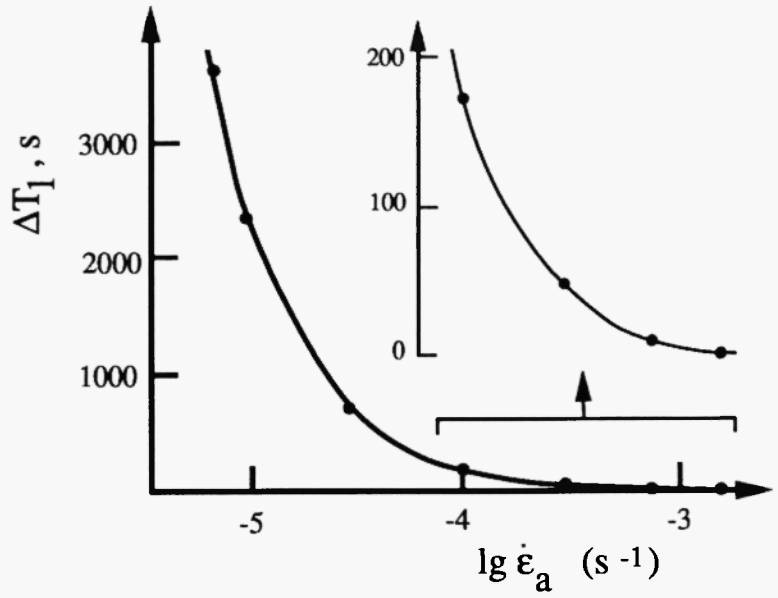

Fig. 16. Reloading time ΔT_1 as a function of imposed strain rate (computed).

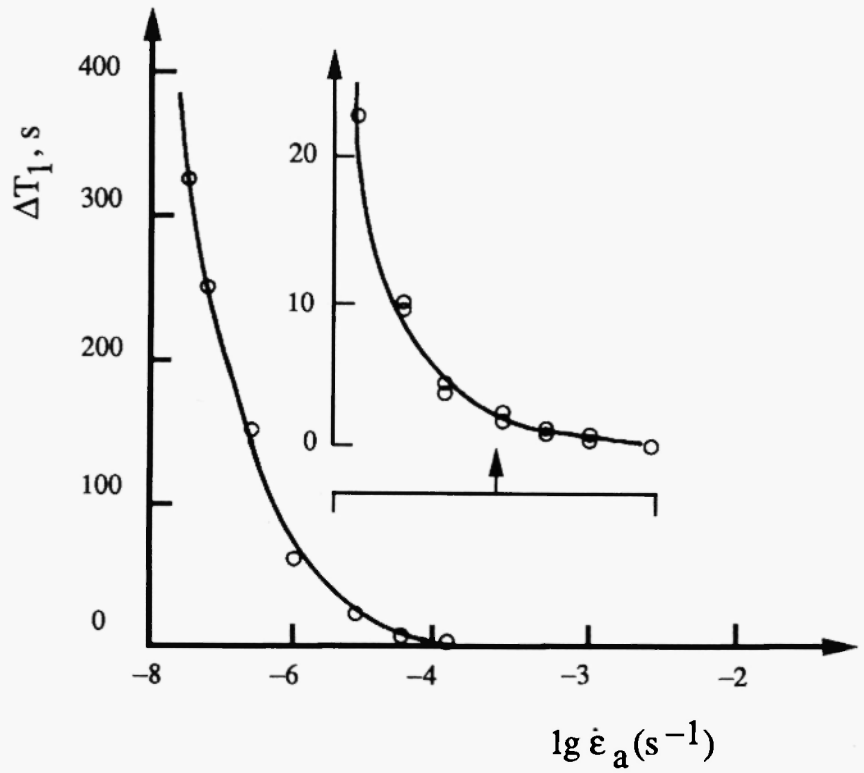

Fig. 17. Reloading time ΔT_1 as a function of imposed strain rate measured on Al–5%Mg [42].

Concluding this section we would like to mention the effect of static recovery which modifies the instability conditions discussed in Sect. 3. It can be shown that in all expressions the stress rate $\dot{\sigma}_0$ has to be replaced by $\dot{\sigma}_0 + r$ where r denotes the phenomenological recovery coefficient in the Bailey–Orowan sense [11]. An interesting result is that at zero stress rate, i.e. in a conventional creep test, the conditions for the occurrence of the PLC effect (in the form of strain bursts),

$$\dot{\epsilon}_1 < r/h < \dot{\epsilon}_2, \tag{34}$$

may be satisfied. This suggests a possible explanation of repeated strain bursts observed in creep, e.g. [52,53].

5. Band velocity

As already mentioned, there is a direct correspondence between the appearance of a stress–strain curve and the features of the corresponding deformation band pattern. Using eqs. (26) and (27) the temporal behaviour (relaxation oscillations of plastic strain rate) depicted on Fig. 5 can trivially be recalculated into the spatial behaviour, provided that the band velocity V is known. Since the latter quantity does not follow from the model, additional considerations have to be invoked.

A plausible assumption would be to postulate that V is related to the dislocation velocity or to the plastic strain rate at the front of a moving band [54–56]. Alternately, it has been assumed [2,11] that the band velocity is proportional to the magnitude of the strain rate jump at the band front $V = \alpha(\dot{\epsilon}_1^* - \dot{\epsilon}_1)$. The proportionality constant α (which is generally temperature dependent) remains an adjustable parameter of the model. It should be noted that neither the period ΔT of relaxation osciallations nor the band propagation velocity V depend on gauge length L (cf. Fig. 6) and the spatial period Λ given by

eq. (26) is generally incommensurate with the latter. Consequently, one band, or several bands, or no band at all may be propagating in the specimen at a given moment.

In an effort to obtain the band velocity from a Penning–type model by including spatial interactions, Zbib and Aifantis [57] heuristically introduced a term proportional to the second derivative of strain with respect to coordinate x along the specimen axis on the right–hand side of Penning's equation, eq. (24). This term, which has the dimensionality of stress, is supposed to take into account the influence of long–range stresses on the initiation of slip ahead of a moving band. The present authors [39,58], as well as Bréchet and Louchet [59] rather treat the problem by considering exchange of mobile dislocations between adjacent elements of material via cross–slip mechanism. This results in the appearance of a "diffusion–like" term $\chi\partial^2\epsilon/\partial x^2$ in the Penning–type equation (21):

$$\sigma = h\epsilon + F(\dot{\epsilon} - \chi\partial^2\epsilon/\partial x^2). \tag{35}$$

Of course, the similarity with diffusion is merely formal, and the analogue of diffusion coefficient, $\chi = \Gamma a^2$, is related to cross–slip parameters: Γ is the cross–slip probability and a denotes a typical cross–slip length.

At first glance, this modification should be sufficient to solve the problem of band velocity determination. Indeed, the physical mechanism of transmission of plastic activity from one specimen site to another is related to cross–slip, and – if deformation band propagation with constant speed turns out to be possible – it should be determined by χ. It can be demonstrated, however, that a travelling wave solution of the type $\epsilon = \epsilon(x–vt)$ is still possible with an arbitrary velocity V. One is again confronted with the problem of selecting the unique velocity which the specimen chooses at given deformation conditions. For systems where a periodic pattern continuously emerges from a uniform steady–state at a bifurcation point, there are several procedures for picking up a unique, physically

distinguished propagation velocity (see [60] for a review). The simplest method based on the Marginal Stability Hypothesis (MSH), was proposed by Dee and Langer [61]. It consists in substance in selecting the velocity for which the moving front is insensitive to fluctuations, whatever their wave number.

Although a formal application of the MSH to the Penning model, extended by a "diffusion–like" term [57], leads to a selected band propagation velocity, the behaviour of this velocity,

$$c = 2\,[h\chi/(dF/d\dot{\epsilon})|_{\dot{\epsilon}=\dot{\epsilon}_s}]^{1/2} \tag{36}$$

with the stress rate is in conflict with experiment. Indeed, c diverges at the boundaries of the PLC interval, $\dot{\epsilon}_s = \dot{\epsilon}_1$, $\dot{\epsilon}_s = \dot{\epsilon}_2$, where $dF/d\dot{\epsilon}$ vanishes. By contrast, Karimi's experiments, [51] show a monotonic decrease of the PLC band velocity V with increasing stress rate (Fig. 18). This discrepancy arises from the fact that PLC instabilities do not belong to the class of phenomena where the procedures mentioned above can apply. Indeed, it can

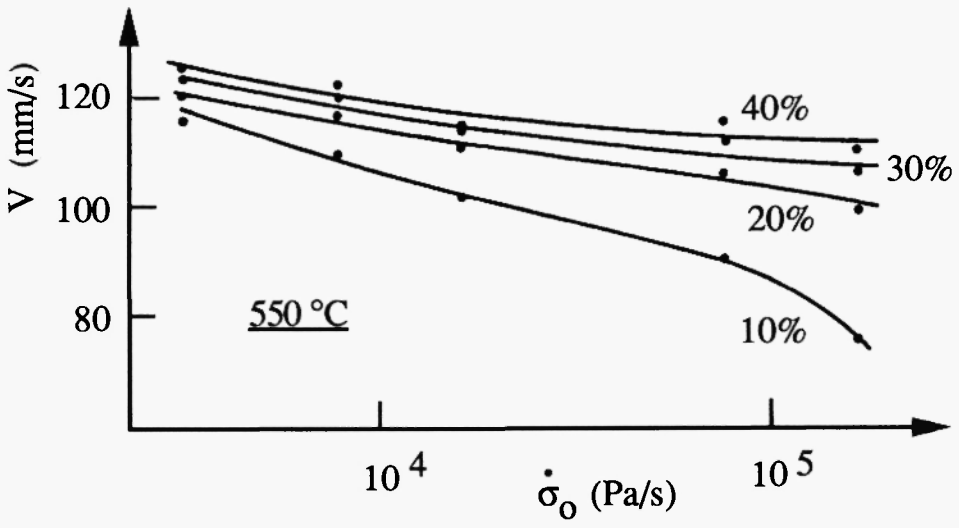

Fig. 18. Stress rate dependence of the PLC band velocity in an austenitic stainless steel. (After Karimi [51]).

be seen from Fig. 4 that the cycle of relaxation oscillations is never infinitesimally close to the steady state value lying along the unstable branch of the characteristic curve, so that linear expansions around the steady state may lead to uncertain results. The problem of velocity selection for a nonlinear differential equation of the generalized relaxation oscillation type (i.e. involving both time and space as variables) still remains to be solved in a general mathematical form although it seems proven that a unique stable velocity does exist. In the absence of analytic tools, computer simulations are required.

6. Concluding remarks

The Portevin–Le Châtelier effect, although known to metallurgists for a long time, was not really understood in its complexity until recently. Its negative practical consequences, such as the occurrence of undesired surface markings, reduced ductility and diminished fracture toughness, observed, in particular, on modern Al– and Ti–based alloys for medium temperature applications, caused an increased activity on the theoretical part. A constitutive model emerged which adequately describes the unstable mechanical response, associated with the PLC effect, on the basis of behaviour of crystal lattice defects. The most significant features of the model have been outlined in the above exposition. It has been shown that the two most important relevant aspects of defect behaviour, viz. dynamic strain ageing and the collective dislocation effects determining the evolution of the dislocation densities, can be efficiently integrated in a rather simple constitutive equation of the Penning type. An additional component of the model is the inclusion of rate effects. Further elements can be introduced if a particular feature of the PLC effect is to be described in more detail, but the most significant phenomena are already covered by the present form of the model.

Some of characteristic properties of the PLC effect, such as the distinction between different types of serrations (A,B,C, etc. [5]), the angle at which the bands are inclined

with respect to the specimen axis, and some others, have not been considered, in order not to depart from the major line of our treatment. We would like to recapitulate it now. The description on the level of lattice defects has led us to a macroscopic model whose mathematical form yields temporal behaviour at a given location (relaxation oscillations in strain rate). Then, a spatial band pattern has been derived via the band propagation velocity V. This is a key quantity in describing the characteristics of the spatial pattern, such as the band spacing and the band width. Determining V from the model, in its extended form, remains a most pressing fundamental problem, and future efforts will undoubtedly concentrate on it.

Acknowledgements

The authors would like to express their thanks to Dr. K. Chihab and Dr. A. Karimi for permission to reproduce some of their unpublished data and to Dr. A. Styczynski for his help with experiments on Al–Li. Financial support from DAAD and ANRT through the PROCOPE program is gratefully acknowledged.

References

1. H. Neuhäuser, this volume.
2. U.F. Kocks, Progr. Mater. Sci., Chalmers anniversary vol. (Pergamon Press, Oxford, 1981) p.185.
3. J.–L. Strudel, in Dislocations et déformation plastique, P. Groh et al., eds. (Les Editions de Physique, 1980) p.199.
4. P. Rodriguez, Bull. Mater. Sci. 6 (1984) p.653.
5. E. Pink and A. Grinberg, Aluminium 60 (1984) 687, 764.
6. F. Le Chatelier, Rev. de Métallurgie 6 (1909) 914.
7. A. Portevin, F. Le Chatelier, Trans. ASST 5 (1924) 457.
8. E.D. Hall, Yield point phenomena in metals and alloys (McMillan, 1970).
9. E. Pink, Strength of metals and alloys, P.O. Kettunen, T.K. Lepistö, and M.E. Lehtonen, eds. (Pergamon Press, Oxford, 1988), vol.1, p.494.
10. S.H. van den Brink, A. van den Beukel, and P.G. McCormick, phys. stat. sol.(6) 30 (1975) 469.

11. L.P. Kubin and Y. Estrin, Acta Metall. 33 (1985) 397.
12. L.P. Kubin and Y. Estrin, Scripta Metall. 23 (1989) 815.
13. P.G. McCormick, Acta Metall. 36 (1988) 3061.
14. A.H. Cottrell, Dislocations and plastic flow in solids (Clarendon Press, Oxford, 1953).
15. J. Friedel, Dislocations (Pergamon Press, Oxford, 1967).
16. P.G. McCormick, Acta Metall. 20 (1972) 35.
17. A. van den Beukel, phys. stat. sol. (a) 30 (1975) 197.
18. C.F. Elam, Proc. R. Soc. London A65 (1938) 568.
19. M.J. Manjoine, Trans. Am. Soc. Min. Engrs. 66 (1944) A211.
20. A.W. Sleeswijk, Acta Metall. 6 (1958) 598.
21. S.R. Bodner, Mater. Sci. and Engg. 2 (1967) 213.
22. S.R. Bodner and A. Rosen, J. Mech. Phys. Solids 15 (1967) 47, 63.
23. P. Penning, Acta Metall. 20 (1972) 1169.
24. L.P. Kubin and Y. Estrin, Strength of metals and alloys, H. McQueen et al., eds. (Pergamon Press, Oxford, 1985) p.331.
25. L.P. Kubin and Y. Estrin, J. Physique 47 (1986) 497.
26. R.A. Mulford and U.F. Kocks, Acta Metall. 27 (1979) 1125.
27. P. Wycliffe, U.F. Kocks, and J.D. Embury, Scripta Metall. 14 (1980) 1349.
28. A. van den Beukel and U.F. Kocks, Acta Metall. 30 (1982) 1027.
29. U.F. Kocks, R.E. Cook, and R.A. Mulford, Acta Metall. 33 (1985) 623.
30. A.H. Cottrell and B.A. Bilby, Proc. Phys. Soc. Conf. B62 (1949) 229.
31. N. Lowat, Scripta Metall. 15 (1981) 1167.
32. A. van den Beukel, Acta Metall. 28 (1980) 965.
33. L.P. Kubin and Y. Estrin, Acta Materialia (in print).
34. Y. Estrin and L.P. Kubin, Acta Metall. 34 (1986) 2455.
35. Y. Estrin and L.P. Kubin, Res Mechanica 23 (1988) 197.
36. A.A. Andronov, A.A. Vit, and C.E. Khaikin, Theory of oscillations (Pergamon Press, Oxford, 1966).
37. M.P. Shaw, H.L. Grubin, and P.R. Solomon, The Gunn–Hilsum effect (Academic Press, New York, 1979).
38. R.F. Cook, M.D. Thouless, D.R. Clarke, Scripta Metall. 23 (1989) 1725.
39. L.P. Kubin and J.P. Poirier in: Nonlinear phenomena in materials science, L.P. Kubin and G. Martin, eds. (Trans. Tech. Publ., Aedermannsdorf, Switzerland, 1988) p.473.
40. L.P. Kubin, K. Chihab, and Y. Estrin, in: Patterns, defects, and microstructures in nonequilibrium systems. Applications in materials science, D. Walgraef, ed. (Martinus Nijhoff Publ., Dordrecht, 1987) p.220.
41. L.J. Cuddy and W.L. Leslie, Acta Metall. 20 (1972) 1157.
42. K. Chihab, Y. Estrin, L.P. Kubin, and J. Vergnol, Scripta Metall. 21 (1987) 203.
43. L.P. Kubin, K. Chihab, and Y. Estrin, Acta Metall. 36 (1988) 2707.
44. W. Räuchle, O.Vöhringer, and E. Macherauch, Mater. Sci. Engg. 12 (1973) 147.
45. P.G. McCormick, in: Formability and metallurgical structure, A.K. Sachdev and J.D. Embury, eds., (TMS–AIME, Philadelphia, 1987), p.227.
46. S. Miura, in: Mechanical behaviour of materials (The Society of Materials Science, Japan, 1972), Vol.1, p.128.
47. J. Guillot and J. Grilhé, Acta Metall. 20 (1972) 291.
48. P.G. McCormick, Scripta Metall. 6 (1972) 165.
49. E. Pink and A. Grinberg, Mater. Sci. Engg. 51 (1981) 1.
50. R.W. Hayes and W.C. Hayes, Acta Metall. 32 (1984) 259.
51. A. Karimi, Doctoral thesis (Ecole des Mines de Paris, 1981).
52. J. Kariya, H. Oikawa, and S. Karashima, Trans. Jap. Inst. of Metals 14 (1973).
53. R.L. Kluck, Mater. Sci. Engg. 54 (1982) 65.

54. G.T. Hahn, Acta Metall. 10 (1962) 727.
55. S.R. Bodner and J. Baruch, J. Appl. Phys. 43 (1972) 2092.
56. M.A. Fortes, J. Mater. Sci. 19 (1984) 1496.
57. H.M. Zbib and E.C. Aifantis, Scripta Metall. 22 (1988) 1331.
58. Y. Estrin, in: Nonlinear phenomena in materials science, L.P. Kubin and G. Martin, eds. (Trans Tech Publ., Aedermannsdorf, Switzerland, 1988) p.417.
59. Y. Bréchet and F. Louchet, ibidem, p.347.
60. Ch. Schiller, Doctorate thesis (Université Libre de Bruxelles, 1989).
61. G. Dee and J.S. Langer, Phys. Rev. Letters 50 (1983) 383.